

# S<sup>2</sup>Mamba: A Spatial-spectral State Space Model for Hyperspectral Image Classification

Guanchun Wang<sup>1</sup>   Xiangrong Zhang<sup>1\*</sup>   Zelin Peng<sup>2</sup>  
 Tianyang Zhang<sup>1</sup>   Xiuping Jia<sup>3</sup>   Licheng Jiao<sup>1</sup>

<sup>1</sup> School of Artificial Intelligence, Xidian University

<sup>2</sup> MoE Key Lab of Artificial Intelligence, Shanghai Jiao Tong University

<sup>3</sup> School of Engineering and Information Technology, University of New South Wales

## Abstract

Land cover analysis using hyperspectral images (HSI) remains an open problem due to their low spatial resolution and complex spectral information. Recent studies are primarily dedicated to designing Transformer-based architectures for spatial-spectral long-range dependencies modeling, which is computationally expensive with quadratic complexity. Selective structured state space model (Mamba), which is efficient for modeling long-range dependencies with linear complexity, has recently shown promising progress. However, its potential in hyperspectral image processing that requires handling numerous spectral bands has not yet been explored. In this paper, we innovatively propose **S<sup>2</sup>Mamba**, a spatial-spectral state space model for hyperspectral image classification, to excavate spatial-spectral contextual features, resulting in more efficient and accurate land cover analysis. In S<sup>2</sup>Mamba, two selective structured state space models through different dimensions are designed for feature extraction, one for spatial, and the other for spectral, along with a spatial-spectral mixture gate for optimal fusion. More specifically, S<sup>2</sup>Mamba first captures spatial contextual relations by interacting each pixel with its adjacent through a Patch Cross Scanning module and then explores semantic information from continuous spectral bands through a Bi-directional Spectral Scanning module. Considering the distinct expertise of the two attributes in homogenous and complicated texture scenes, we realize the Spatial-spectral Mixture Gate by a group of learnable matrices, allowing for the adaptive incorporation of representations learned across different dimensions. Extensive experiments conducted on HSI classification benchmarks demonstrate the superiority and prospect of S<sup>2</sup>Mamba. The code will be available at: <https://github.com/PURE-melo/S2Mamba>.

## 1 Introduction

Hyperspectral images (HSI), consisting of numerous spectral bands, are capable of land cover analysis due to their rich material information [1, 2, 3, 4], with extensive application in domains such as precision agriculture, mineral exploration, and environmental monitoring [5, 6]. Therefore, there is a strong incentive to design a more effective and efficient model for hyperspectral image classification. Convolutional neural networks (CNNs) [7, 8, 9, 10, 11] as a widespread paradigm have been widely studied in hyperspectral image classification. However, this paradigm is limited by its local receptive fields and is unable to comprehensively capture continuous spectral properties. Transformer architectures [12, 13, 14, 15, 16, 17] have been recently explored in hyperspectral image classification, which exhibits remarkable performance due to their ability to extract global contextual information on both spatial and spectral dimensions.

\*Correspondence to: <gwwang\_2@stu.xidian.edu.cn, xrzhang@mail.xidian.edu.cn>

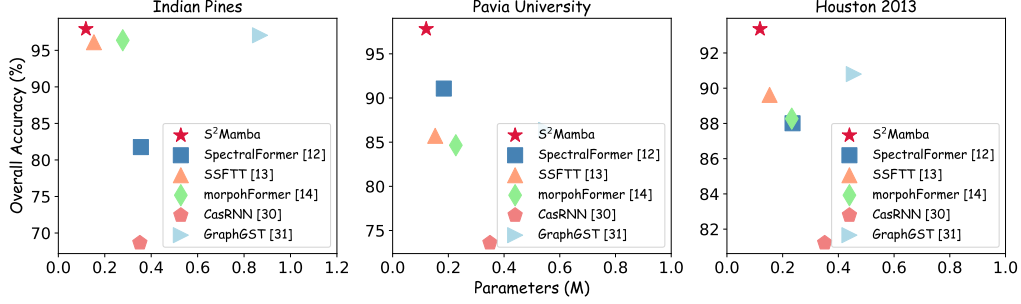


Figure 1: Overall Accuracy (%) and Parameters (M) comparison on Indian Pines, Pavia University, Houston 2013 dataset. Our proposed S²Mamba achieves optimal results in terms of overall accuracy and parameters compared to existing methods [12, 13, 14, 30, 31].

Despite its powerful representation ability, dealing HSI data with transformer-based models is computationally expensive, primarily due to the self-attention mechanism with quadratic computational complexity  $\mathcal{O}(N^2)$  [18, 19]. As an efficient alternative to self-attention mechanisms, the selective structured state space model (Mamba) [20] has recently emerged as a powerful tool with linear complexity for modeling long-range dependency in sequence processing. Derived from this, a series of Mamba-based models [21, 22, 23, 24, 25, 26, 27, 28, 29] have been explored for various computer vision tasks, such as image classification, semantic segmentation, and others. However, most of these models are only applied in natural image processing, leaving a blank in hyperspectral image classification due to the difficulty in handling complicated spatial-spectral information.

Drawing inspiration from the success of state space models, this paper seeks to explore their potential for HSI processing. To this end, we propose a spatial-spectral state space model (S²Mamba) to jointly excavate long-range spatial relations and continuous spectral features for hyperspectral image classification. Our S²Mamba comprises **Patch Cross Scanning** and **Bi-directional Spectral Scanning** modules for capturing spatial and spectral information, respectively, and merging them with a **Spatial-spectral Mixture Gate**. Specifically, we build a patch cross scanning mechanism to capture the contextual relations between adjacent pixels, wherein the patch data is first flattened into pixel sequences through different route generation ways and a selective structured state space model is then applied to these sequences for capturing contextual features. Considering the rich knowledge within continuous spectral bands, we design an extra scanning module on the spectral dimension for retrieving semantic properties in HSI data by a bi-directional interaction between each band.

The remaining dilemma lies in optimally merging spatial and spectral attributes of HSI data. We observe that spectral information exhibits a more significant role for uniform land cover regions than those regions with complex textures. This is due to the paucity of spatial cues within homogenous regions, necessitating the reliance on spectral information for determining land cover categories. In contrast, spatial information can offer a considerable prior in dealing with regions containing complex textures, thereby enhancing classification performance. To address this, we here propose a spatial-spectral mixture gate to dynamically merge the above features pixel by pixel, wherein each spatial location is assigned a group of learnable weights to determine the ratio of various features. This gating mechanism, promoting the competition of the two features, facilitates the integration of spatial-spectral attributes by truncating those redundant ones, greatly boosting the accuracy.

Through experimental assessment, we verify the effectiveness of S²Mamba on the three public hyperspectral image classification datasets. Fig. 1 illustrates that our S²Mamba improves the previous SOTA method by 0.86%, 6.74%, and 2.56% in terms of overall accuracy on Indian Pines, Pavia University, and Houston 2013 datasets, respectively. Meanwhile, it outperforms Transformer-based models with the fewest parameters (about 0.12M) and a linear complexity  $\mathcal{O}(kN)$ , where  $k \ll N$ .

## 2 Related Work

### 2.1 Hyperspectral Image Classification

Existing methods typically solve the hyperspectral image classification problem by leveraging well-crafted deep neural networks, which can be primarily divided into several categories: convolutional

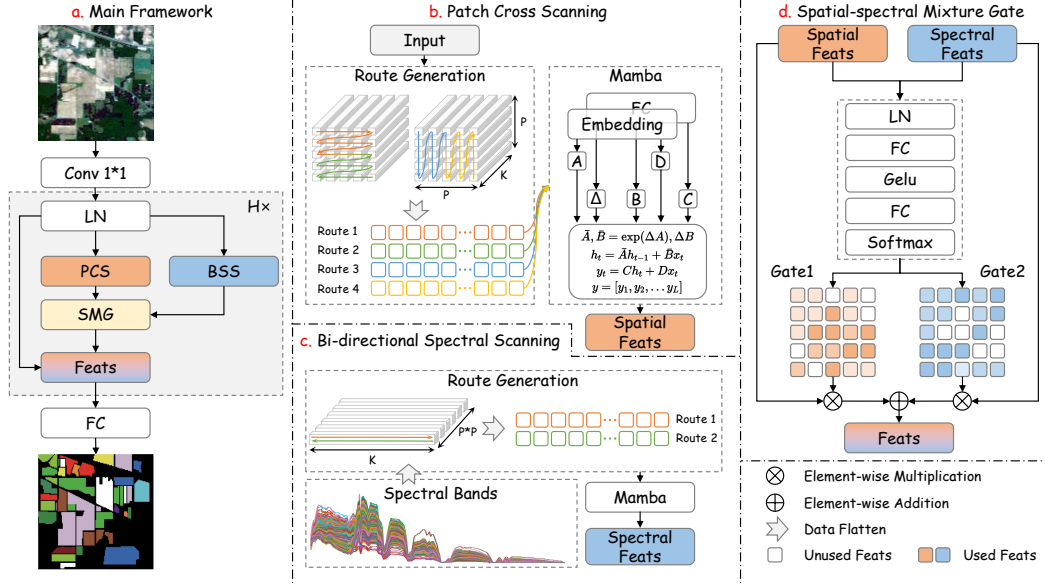


Figure 2: Illustration of our proposed S<sup>2</sup>Mamba, consisting of a patch cross scanning (PCS) mechanism, a bi-directional spectral scanning (BSS) mechanism, and a spatial-spectral mixture gate (SMG).

neural network-based [8, 9, 32, 33, 34, 35, 36, 7, 37, 38, 10, 11, 39, 40, 41, 42], recurrent neural network-based [43, 44, 30], and Transformer-based [45, 13, 15, 16, 12, 14, 17, 46, 47, 31, 48].

**Traditional Models.** CNNs are widely applied in hyperspectral classification tasks, an excellent feature extraction architecture that captures spatial and local semantic information. Recent works have explored CNNs to individually extract spatial [36, 7] and spectral features [37, 38] from hyperspectral remote sensing images, or to learn spatial-spectral joint representation [8, 9, 32, 33, 34, 35], achieving remarkable progress. Considering that CNN structures are incapable of modeling irregular data, some research introduced graph convolutional networks (GCNs) [10, 11, 39, 40] to mine the potential spatial semantic information of HSI data. Another group of studies serves the spectral information across different bands of HSI data as continuous sequences and employs recurrent neural networks (RNNs) [43, 44, 30] to extract spectral features for classification. However, these methods often struggle to extract global spectral information due to their limited capability in long-range dependency.

**Transformer-based Models.** Transformer is a powerful architecture consisting of multiple self-attention mechanisms to extract global contextual information, and currently, they have been explored for hyperspectral image classification. Most of these methods [45, 13, 15, 16, 12, 14, 17, 46, 47, 31, 48] attempt to learn the global sequential information on both spatial and spectral dimensions. Spectralformer [12] is the first one in its kind to introduce the Transformer architecture into hyperspectral image classification, which jointly captures the local and global information by grouping the adjacent bands. Beyond single Transformer structures, some methods adopt hybrid networks to acquire spatial-spectral features. SSFTT [13] utilizes convolutional layers to describe the low-level features and integrate them through Transformer layers. morphFormer [14] uses morphological convolution layers to learn both spatial and spectral representations and merges them by applying Transformer layers. Besides, other works [48] incorporate RNNs with Transformers to collaboratively extract continuous spectral features and spatial context features, significantly enhancing the classification performance.

Unlike previous methods that capture long-range dependencies by compute-intensive Transformer structures, we innovatively explore a fully sequential architecture based on selective structured state space models for efficient global spatial-spectral feature extraction.

## 2.2 State Space Models

Most recently, state space models (SSMs) [49, 50, 51, 52, 53], especially the structured state space models (S4) [50] have shown promising progress in sequence analysis, which are capable of long-

range sequence modeling with linear computational complexity. By introducing a selective mechanism into [50], Mamba [20] further optimizes its context compression ability and exhibits superior performance to Transformers. Considering its outstanding performance in sequence data processing, many works have explored the potential of Mamba [20] in computer vision and achieved promising advancements. In particular, visual state space model (Vmamba) [22] and vision Mamba (Vim) [21] have recently emerged as powerful tools for various computer vision tasks due to their efficiency in modeling long-range dependencies. On the basis of them, a series of visual state space models have been proposed, such as medical image analysis [25, 27, 54, 55], video understanding [28, 56], and others [26, 24, 57, 29, 58, 23]. However, most of these methods are only applied in RGB images, leaving a blank in hyperspectral image classification that requires handling complex spectral information. Thus, we propose a Mamba-based architecture for hyperspectral image classification, fully exploiting spatial-spectral features by state space models.

### 3 Proposed Method

#### 3.1 Preliminaries

**State Space Models.** State space models are foundational statistical models that describe the dynamic behavior of systems and are widely applied in domains such as time series analysis and control systems. In SSMs, the continuous evolution of systems is calculated through a set of ordinary differential equations (ODEs), which map an input signal into a latent space and decode it into an output sequence. This operation can be defined as:

$$\begin{aligned} h'(t) &= \mathbf{A}h(t) + \mathbf{B}x(t) \\ y(t) &= \mathbf{C}h(t) + \mathbf{D}x(t) \end{aligned} \quad (1)$$

where  $h(t) \in \mathbb{R}^N$ ,  $x(t) \in \mathbb{R}$ , and  $y(t) \in \mathbb{R}$  indicate latent state, input signal, and output signal, respectively.  $h'(t) \in \mathbb{R}^N$  refers to the time derivative of  $h(t)$ .  $N$  and  $L$  represent the dimensions of the latent space and sequences, respectively. Additionally,  $\mathbf{A} \in \mathbb{R}^{N \times N}$  is the state transition matrix.  $\mathbf{B} \in \mathbb{R}^N$  and  $\mathbf{C} \in \mathbb{R}^N$  are projection matrices.  $\mathbf{D}$  is usually served as a residual connected operation and thus discarded in the equation. To facilitate the integration of continuous state space models with discrete sequences, Mamba [20] employs a zero-order hold technique to discretize the ordinary differential equations as follows:

$$\begin{aligned} \overline{\mathbf{A}} &= \exp(\Delta \mathbf{A}) \\ \overline{\mathbf{B}} &= (\Delta \mathbf{A})^{-1}(\exp(\Delta \mathbf{A}) - \mathbf{I}) \cdot \Delta \mathbf{B} \end{aligned} \quad (2)$$

where  $\overline{\mathbf{A}}$  and  $\overline{\mathbf{B}}$  represent the discretized forms of the parameters  $\mathbf{A}$  and  $\mathbf{B}$ , respectively, through a discretization step size  $\Delta$ . As stated in [20], the projection matrix  $\overline{\mathbf{B}}$  can be approximated using the first-order Taylor series:

$$\overline{\mathbf{B}} = (\exp(\mathbf{A}) - \mathbf{I})\mathbf{A}^{-1}\mathbf{B} \approx (\Delta \mathbf{A})(\Delta \mathbf{A})^{-1}\Delta \mathbf{B} = \Delta \mathbf{B} \quad (3)$$

After discretization, the ODEs of SSMs can be represented as follows:

$$\begin{aligned} h_t &= \overline{\mathbf{A}}h_{t-1} + \overline{\mathbf{B}}x_t \\ y_t &= \mathbf{C}h_t \end{aligned} \quad (4)$$

**Selective Scan Mechanism.** Traditional SSMs are linear time-invariant, i.e., the projection matrices do not vary with input signals, resulting in non-selective attention on each sequence unit. To alleviate this, Mamba [20] modifies the parameter matrices to be input-dependent, i.e.,  $\mathbf{B} \in \mathbb{R}^{B \times L \times N}$ ,  $\mathbf{C} \in \mathbb{R}^{B \times L \times N}$  and  $\Delta \in \mathbb{R}^{B \times L \times D}$  are calculated based on  $\mathbf{X} \in \mathbb{R}^{B \times L \times D}$ , further improving the ability for handling complex sequences by transforming the SSMs into linear time-varying systems.

#### 3.2 S<sup>2</sup>Mamba

Fig. 2 shows the overall architecture of our proposed S<sup>2</sup>Mamba framework for hyperspectral image classification. The input data is first fed into a convolutional layer for embedding and then fed into patch cross scanning and bi-directional scanning modules to capture spatial and spectral features.

Finally, the above terms are fused by a spatial-spectral mixture gate for category prediction. Unlike recent advanced approaches that utilize Transformer-based networks with quadratic complexity to capture global spatial-spectral features, our S<sup>2</sup>Mamba is a powerful spatial-spectral information extraction network with linear computational complexity.

### 3.2.1 Patch Cross Scanning Mechanism

To facilitate the selective scanning mechanism with HSI inputs, we first extend the vanilla selective scan mechanism [20, 22] to the patch-level HSI data and design a patch cross scanning mechanism, which captures spatial contextual relations by interacting each pixel with its adjacent through a state space model. Given the input of HSI patch  $\mathbf{X} \in \mathbb{R}^{P \times P \times K}$ , where  $P$  and  $K$  denote the patch size and spectral band number of the data cube, respectively, we perform a pixel-by-pixel scanning strategy on four different routes. As illustrated in Fig. 2, each route is generated from different directions, such as top to bottom, left to right, and vice versa.

More specifically, we first flatten the patch data into one-dimensional sequences with the preset routes, and then recurrently calculate each item of sequences  $\mathcal{X}_{\text{seq}} = \{[\mathbf{x}_0^i, \mathbf{x}_1^i, \dots, \mathbf{x}_{P \times P}^i] \mid \mathbf{x}_j^i \in \mathbb{R}^{1 \times K}, i \in \{0, 1, 2, 3\}\}$  by using rewritten Eq. (4):

$$\begin{aligned} \mathbf{h}_j^i &= \overline{\mathbf{A}}_{\text{spa}} \mathbf{h}_{j-1}^i + \overline{\mathbf{B}}_{\text{spa}} \mathbf{x}_j^i \\ \mathbf{y}_j^i &= \mathbf{C}_{\text{spa}} \mathbf{h}_j^i + \mathbf{x}_j^i \end{aligned} \quad (5)$$

where  $\overline{\mathbf{A}}_{\text{spa}}$ ,  $\overline{\mathbf{B}}_{\text{spa}}$  and  $\overline{\mathbf{C}}_{\text{spa}}$  represent the trainable parameters in PCS. After scanning, we can obtain a set of output sequences  $\mathcal{Y}_{\text{seq}} = \{[\mathbf{y}_0^i, \mathbf{y}_1^i, \dots, \mathbf{y}_{P \times P}^i] \mid \mathbf{y}_j^i \in \mathbb{R}^{1 \times K}, i \in \{0, 1, 2, 3\}\}$ . Next, the output sequences obtained from different scanning routes are fused according to the operations in Fig. 2, such as flipping or transposing sequences. As a result, each element in the output sequence  $\mathbf{Y} \in \mathbb{R}^{P \times P \times K}$  can integrate influences with its adjacent regions from different directions.

### 3.2.2 Bi-directional Spectral Scanning Mechanism

Although the above scanning mechanism involves the spatial contextual information within the data cube, it lacks consideration for continuous spectral band information inherent in HSI data. One naive approach to address this issue is to scan the data cube band by band, capturing the semantic cues from rich spectral bands. However, due to the unidirectional information induction attribute of state space models, the spectral scanning mechanism conducted in a single direction may fail to adequately capture the contextual information between spectral bands, leading to limited spectral utilization.

To this end, we further design a bi-directional spectral scanning mechanism, analyzing the varying tendency of the continuous spectrum from multiple directions by scanning spectral dimension band by band. We first flatten the HSI patch along the spatial dimensions to acquire the data matrix  $\mathbf{S} \in \mathbb{R}^{K \times P^2}$ , and then recurrently calculate each item of sequences  $\mathcal{S}_{\text{seq}} = \{[\mathbf{s}_0^i, \mathbf{s}_1^i, \dots, \mathbf{s}_K^i] \mid \mathbf{s}_j^i \in \mathbb{R}^{1 \times P^2}, i \in \{0, 1\}\}$  by following operation:

$$\begin{aligned} \tilde{\mathbf{h}}_j^i &= \overline{\mathbf{A}}_{\text{spe}} \tilde{\mathbf{h}}_{j-1}^i + \overline{\mathbf{B}}_{\text{spe}} \mathbf{s}_j^i \\ \mathbf{p}_j^i &= \mathbf{C}_{\text{spe}} \tilde{\mathbf{h}}_j^i + \mathbf{s}_j^i \end{aligned} \quad (6)$$

where  $\mathbf{p}_j^i$  denotes the  $j$ th element in the  $i$ th order of output sequences.  $\overline{\mathbf{A}}_{\text{spe}}$ ,  $\overline{\mathbf{B}}_{\text{spe}}$  and  $\overline{\mathbf{C}}_{\text{spe}}$  represent the trainable parameters in BSS. After scanning, we can obtain a set of output sequences  $\mathcal{P}_{\text{seq}} = \{[\mathbf{p}_0^i, \mathbf{p}_1^i, \dots, \mathbf{p}_K^i] \mid \mathbf{p}_j^i \in \mathbb{R}^{1 \times P^2}, i \in \{0, 1\}\}$ . Next, the output sequences  $\mathbf{P} \in \mathbb{R}^{P \times P \times K}$  are fused from different routes, which integrate influences from adjacent bands into each spectral band, further boosting its discriminative ability.

### 3.2.3 Spatial-spectral Mixture Gate

After acquiring the spatial and spectral information of HSI through the two scanning modules, calculating the optimal mixture representation becomes a key challenge. As discussed in Sec. 1, the effectiveness of spatial and spectral features in HSI classification differs across different scenarios, thereby their direct merging without prior may lead to contradictions.

Specifically, we note that spectral information acts more prominence in the classification of uniform regions as opposed to those characterized by complicated textures. This is attributable to the scarcity

Table 1: Comparison results (OA%/AA%/κ) on the Indian Pines test set. The best is in bold.

Category	CNNs			RNN		Transformers					Mamba
	1-D CNN	2-D CNN	miniGCN	RNN	CasRNN	ViT	SpectralFormer	morphFormer	SSFTT	GraphGST	S <sup>2</sup> Mamba
1	47.83	65.90	72.54	69.00	61.78	53.25	70.52	93.14	91.18	<b>95.81</b>	94.44
2	42.35	76.66	55.99	58.93	57.78	66.20	81.89	97.70	98.72	98.85	<b>100.00</b>
3	60.87	92.39	92.93	77.17	75.00	86.41	91.30	100.00	100.00	100.00	<b>100.00</b>
4	89.49	93.96	92.62	82.33	90.16	89.71	95.53	96.87	96.19	97.09	<b>98.43</b>
5	92.40	87.23	94.98	67.72	81.35	87.66	85.51	99.86	100.00	98.57	<b>100.00</b>
6	97.04	97.27	98.63	89.07	87.70	89.98	99.32	99.77	100.00	99.54	<b>100.00</b>
7	59.69	77.23	64.71	69.06	79.08	72.22	81.81	86.71	95.10	97.93	<b>98.47</b>
8	65.38	57.03	68.78	63.56	56.29	66.00	75.48	97.93	94.44	94.50	<b>98.10</b>
9	93.44	72.87	69.33	65.07	60.11	57.09	73.76	94.33	90.96	95.04	<b>95.04</b>
10	99.38	100.00	98.77	95.06	95.06	97.53	98.77	100.00	100.00	98.76	<b>100.00</b>
11	84.00	92.85	87.78	88.67	82.23	87.62	93.17	99.12	99.35	<b>99.59</b>	97.67
12	86.06	88.18	50.00	50.00	46.97	63.94	78.48	99.09	100.00	98.48	<b>100.00</b>
13	91.11	100.00	100.00	97.78	97.78	95.56	100.00	100.00	100.00	100.00	<b>100.00</b>
14	84.62	84.62	48.72	66.67	56.41	79.49	79.49	92.31	100.00	100.00	<b>100.00</b>
15	100.00	100.00	72.73	81.82	81.82	90.91	100.00	100.00	100.00	100.00	<b>100.00</b>
16	80.00	100.00	80.00	100.00	100.00	80.00	100.00	100.00	100.00	100.00	<b>100.00</b>
OA (%)	70.43	75.89	75.11	70.66	68.65	71.86	81.76	96.38	96.11	97.06	<b>97.92</b>
AA (%)	79.60	86.64	78.03	76.37	75.59	78.97	87.81	97.30	97.92	98.39	<b>98.88</b>
κ	0.6642	0.7281	0.7164	0.6673	0.6464	0.6804	0.7919	0.9584	0.9555	0.9664	<b>0.9761</b>

Table 2: Comparison results (OA%/AA%/κ) on the Pavia University test set. The best is in bold.

Category	CNNs			RNN		Transformers					Mamba
	1-D CNN	2-D CNN	miniGCN	RNN	CasRNN	ViT	SpectralFormer	morphFormer	SSFTT	GraphGST	S <sup>2</sup> Mamba
1	88.90	80.98	<b>96.35</b>	84.01	77.62	71.51	82.73	89.90	87.64	84.99	96.24
2	58.81	81.70	89.43	66.95	63.41	76.82	94.03	75.26	76.60	82.43	<b>98.75</b>
3	73.11	67.99	<b>87.01</b>	58.46	57.30	46.39	73.66	85.90	85.56	79.94	85.95
4	82.07	97.36	94.26	97.70	98.42	96.39	93.75	86.33	95.54	90.80	<b>97.73</b>
5	99.46	99.64	99.82	99.10	99.37	99.19	99.28	95.87	<b>100.00</b>	100.00	99.10
6	97.92	97.59	43.12	83.18	75.17	83.18	90.75	95.54	98.08	90.66	<b>99.30</b>
7	88.07	82.47	90.96	83.08	88.48	83.08	87.56	98.27	99.18	98.78	<b>99.90</b>
8	88.14	97.62	77.42	89.63	87.25	89.63	95.81	98.01	94.41	93.10	<b>98.93</b>
9	99.87	95.60	87.27	96.48	99.11	96.48	94.21	96.86	98.62	<b>99.25</b>	98.36
OA (%)	75.50	86.05	79.79	77.13	73.60	76.99	91.07	84.65	85.72	86.39	<b>97.81</b>
AA (%)	86.26	88.99	85.07	84.29	82.91	80.22	90.20	91.32	92.85	91.11	<b>97.14</b>
κ	0.6948	0.8187	0.7367	0.7101	0.6677	0.7010	0.8805	0.8162	0.7941	0.8220	<b>0.9705</b>

of spatial cues within homogenous regions, which in turn emphasizes the importance of spectral information for differentiating these land cover. In this case, PCS may contribute to misleading directions as a consequence of the redundant features. Inversely, it offers considerable prior in dealing with regions characterized by complex textures, thereby enhancing the richness of discriminative representation.

To address this, we here propose a spatial-spectral mixture gate to dynamically merge the above features for each position, wherein each location is assigned a group of learnable weights  $\tilde{\mathbf{M}} \in \mathbb{R}^{P \times P \times 2}$  to determine the ratio of various features as follows:

$$\begin{aligned}\tilde{\mathbf{M}}_0 &= \frac{\exp(\mathcal{H}(\mathbf{Y}; \Theta_g))}{\exp(\mathcal{H}(\mathbf{Y}; \Theta_g)) + \exp(\mathcal{H}(\mathbf{P}; \Theta_g))} \\ \tilde{\mathbf{M}}_1 &= \frac{\exp(\mathcal{H}(\mathbf{P}; \Theta_g))}{\exp(\mathcal{H}(\mathbf{Y}; \Theta_g)) + \exp(\mathcal{H}(\mathbf{P}; \Theta_g))}\end{aligned}\quad (7)$$

where  $\mathcal{H}(*; \Theta_g)$  indicates the feature encoder in SMG. It consists of two fully connected layers with a gaussian error linear unit activation function. Next, a softmax activation function is applied to transfer them into probability maps, whose values are between 0 and 1. Subsequently, we merge the above features as follows:

$$\mathbf{F} = (\tilde{\mathbf{M}}_0 \cdot \mathbb{1}(\tilde{\mathbf{M}}_0 > \tau)) \odot \mathbf{Y} + (\tilde{\mathbf{M}}_1 \cdot \mathbb{1}(\tilde{\mathbf{M}}_1 > \tau)) \odot \mathbf{P} \quad (8)$$

where  $\tau$  is the threshold for pruning those low contribution features. By employing this gating mechanism, redundant features that do not contribute to HSI classification can be effectively truncated, facilitating the integration of spatial-spectral attributes. The intuition behind SMG is to encourage competition between the two types of features to select the most discriminative ones under different scenarios, thereby achieving a more satisfactory fusion.



Table 3: Comparison results (OA%/AA%/ $\kappa$ ) on the Houston 2013 test set. The best is in bold.

Category	CNNs			RNN		Transformers					Mamba
	1-D CNN	2-D CNN	miniGCN	RNN	CasRNN	ViT	SpectralFormer	morphFormer	SSFTT	GraphGST	S <sup>2</sup> Mamba
1	87.27	85.09	<b>98.39</b>	82.34	82.62	82.81	81.86	93.63	85.37	85.66	83.10
2	98.21	99.91	92.11	94.27	96.90	96.62	100.00	98.02	99.81	99.91	<b>100.00</b>
3	<b>100.00</b>	77.23	99.60	99.60	99.60	99.80	95.25	99.20	95.05	95.64	99.60
4	92.99	97.73	96.78	97.54	96.97	<b>99.24</b>	96.12	95.64	90.24	91.29	98.20
5	97.35	99.53	97.73	93.28	97.35	97.73	99.53	98.95	100.00	100.00	<b>100.00</b>
6	95.10	92.31	95.10	95.10	95.10	95.10	94.41	100.00	100.00	<b>100.00</b>	95.80
7	77.33	<b>92.16</b>	57.28	83.77	76.21	76.77	83.12	86.66	75.00	76.96	89.37
8	51.38	79.39	68.09	56.03	44.63	55.65	76.73	83.85	89.74	<b>89.84</b>	88.60
9	27.95	86.31	53.92	72.14	64.97	67.42	79.32	75.92	76.86	83.57	<b>92.45</b>
10	90.83	43.73	77.41	84.17	78.28	68.05	78.86	66.50	90.92	91.79	<b>92.57</b>
11	79.32	87.00	84.91	82.83	88.43	82.35	88.71	82.06	87.95	91.46	<b>91.56</b>
12	76.56	66.28	77.23	70.61	66.38	58.50	87.32	87.22	<b>92.02</b>	90.49	90.97
13	69.47	<b>90.18</b>	50.88	69.12	70.53	60.00	72.63	84.91	80.00	81.40	89.12
14	99.19	90.69	98.38	98.79	100.00	98.79	100.00	100.00	100.00	100.00	<b>100.00</b>
15	98.10	77.80	98.52	95.98	96.62	98.73	99.79	99.57	100.00	100.00	<b>100.00</b>
OA (%)	80.04	83.72	81.71	83.23	81.22	80.41	88.01	88.27	89.62	90.80	<b>93.36</b>
AA (%)	82.74	84.35	83.09	85.04	83.64	82.50	88.91	90.15	90.87	91.93	<b>94.09</b>
$\kappa$	0.7835	0.8231	0.8018	0.8183	0.7967	0.7876	0.8699	0.8727	0.8873	0.8853	<b>0.9279</b>

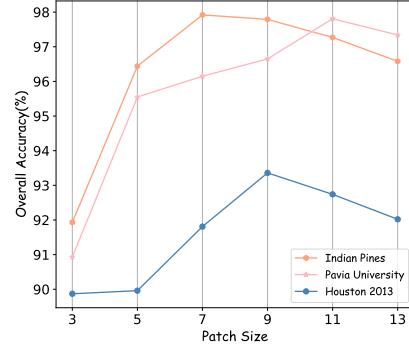
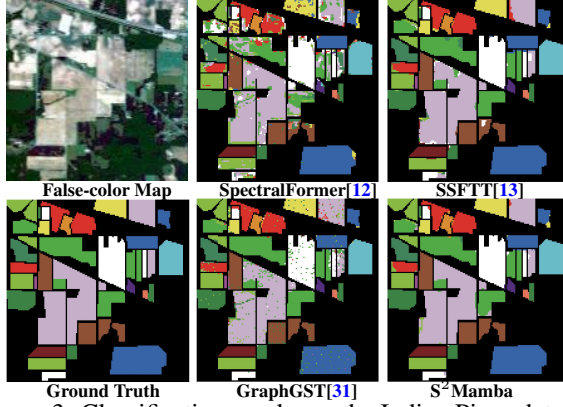


Figure 3: Classification results on the Indian Pines dataset. Figure 4: Parameter analysis of the patch size in S<sup>2</sup>Mamba.

## 4 Experiment

### 4.1 Experimental Setup

**Datasets.** We conduct evaluations of our S<sup>2</sup>Mamba on three publicly available datasets, focusing on hyperspectral image classification: Indian Pines, Pavia University, and Houston 2013 datasets. The Indian Pines dataset consists of  $145 \times 145$  pixels at a ground sampling distance of 20 m and 220 spectral bands spanning the wavelength range of 400–2500 nm, in which 200 spectral bands are preserved after removing 20 noisy and water absorption bands. The dataset is annotated using 16 land cover categories, including crops, trees, and other vegetation. The Pavia University dataset consists of  $610 \times 340$  pixels at a ground sampling distance of 1.3 m and 103 spectral bands spanning the wavelength range of 430 to 860 nm, which is annotated using 9 land cover categories, including asphalt, meadows, gravel, trees, metal sheets, bare soil, bitumen, bricks, and shadows. The Houston 2013 dataset consists of  $349 \times 1905$  pixels at a ground sampling distance of 2.5 m and 144 spectral bands spanning the wavelength range of 380 to 1050 nm. The dataset is annotated using 15 land cover categories, including healthy grass, stressed grass, synthetic grass, trees, soil, water, residential, and others. Notably, all experiments use the *same training and validate samples* as [12] for a fair comparison, which is also detailed in the supplementary materials.

**Evaluation.** To evaluate the classification performance of our S<sup>2</sup>Mamba, we utilized three commonly used evaluation metrics: overall accuracy (OA), average accuracy (AA), and kappa coefficient ( $\kappa$ ).

**Implementation Details.** All the experiments are conducted within the PyTorch framework, utilizing a single NVIDIA GeForce RTX 4090 with 24-GB GPU memory. For the initialization of our S<sup>2</sup>Mamba, its parameters are randomly initialized by a zero-mean normal distribution with a standard deviation of 0.01. AdamW [59] is adopted as the optimizer for S<sup>2</sup>Mamba, where the exponential learning rate strategy is applied with an initial value of 0.0001. The model is trained with 400 epochs, where the batch size is set to 64. The patch size of inputs is set to 7, 11, and 9 for Indian Pines, Pavia University and Houston 2013, respectively. The number of blocks  $N$  is set to 1.

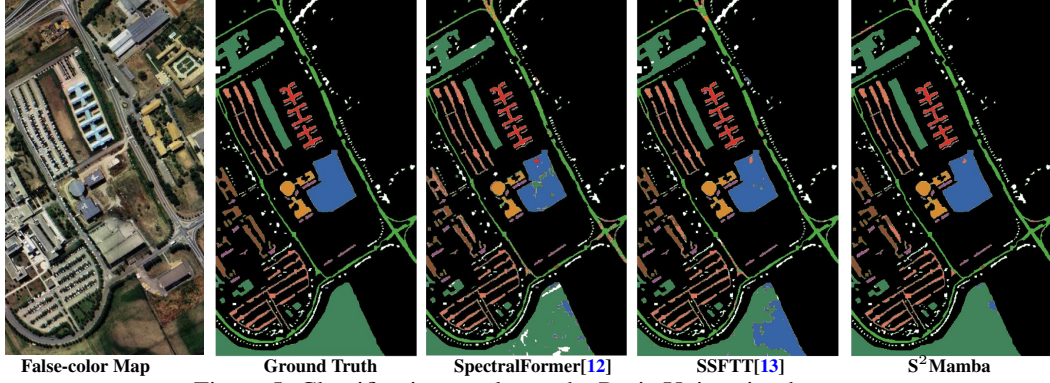


Figure 5: Classification results on the Pavia University dataset.

Table 4: Ablation study on the impact of each component in S²Mamba. "PCS": Patch Cross Scanning. "BSS": Bi-directional Spectral Scanning. "SMG": Spatial-spectral Mixture Gate.

PCS	BSS	SMG	Indian Pines			Pavia University			Houston 2013		
			OA (%)	AA (%)	$\kappa$	OA (%)	AA (%)	$\kappa$	OA (%)	AA (%)	$\kappa$
✓			96.45	97.99	0.9593	96.42	96.53	0.9521	90.78	92.05	0.9002
	✓		96.51	98.27	0.9599	96.24	96.21	0.9493	92.19	93.29	0.9154
✓	✓		97.19	98.56	0.9678	97.17	97.12	0.9620	92.74	93.36	0.9211
✓	✓	✓	<b>97.92</b>	<b>98.88</b>	<b>0.9761</b>	<b>97.81</b>	<b>97.14</b>	<b>0.9705</b>	<b>93.36</b>	<b>94.09</b>	<b>0.9279</b>

## 4.2 Comparison with State-of-the-Arts

We conduct a comprehensive evaluation of our S²Mamba and compare it with several comparative approaches, including CNN-based (1-D CNN, 2-D CNN, miniGCN [11]), RNN-based (RNN, Cas-RNN [30]), and Transformer-based (ViT [19], Spectralformer [12], morphformer [14], SSFTT [13], GraphGST [31]) methods, where 1-D CNN, 2-D CNN, RNN, and ViT are implemented following [12]. All methods are tested using the optimal experimental settings reported in their papers or re-implemented by their official code.

**Indian Pines.** In Table 1, we benchmark performances on the Indian Pines dataset. The results, presented in Table 1, demonstrate that our approach significantly outperforms state-of-the-art hyperspectral image classification methods on 14 categories, achieving the best comprehensive performance in terms of OA (97.92% vs. 97.06%), AA (98.88% vs. 98.39%), and  $\kappa$  (0.9761 vs. 0.9664). In particular, we surpass the performance of the typical Transformer-based method, i.e., SpectralFormer [12], which utilizes transformer architecture to extract long-range dependencies from continuous spectral bands. In contrast, our S²Mamba, involving more efficient basic structures and elaborate designs, achieves superior results in terms of OA, AA, and  $\kappa$  (e.g., improving the OA from 81.76% to 97.92%). Furthermore, Fig. 3 shows examples of prediction maps. It demonstrates that our S²Mamba is capable of producing accurate predictions of each category.

**Pavia University.** We further evaluate our S²Mamba on the Pavia University dataset, whose scenario includes numerous complex spatial textures. As illustrated in Table 2, our method significantly outperforms the comparative techniques with at least 6.74%, 4.29%, and 9.00% in terms of OA, AA, and  $\kappa$ , respectively. This confirms that our S²Mamba can offer a more satisfactory solution under complex scenarios. Fig. 5 shows that our approach achieves superior performance than others with more completed prediction maps, such as asphalt (masked in light green color) and meadow (masked in dark green color).

**Houston 2013.** Furthermore, we compare our proposed method with the state-of-the-art methods on the more challenging dataset, i.e., Houston 2013. The experimental results, presented in Table 3, demonstrate that our S²Mamba significantly outperforms state-of-the-art hyperspectral image classification methods on 8 categories, achieving the best comprehensive performance in terms of OA, AA, and Kappa coefficient. Specifically, it exhibits 2.56%, 2.16%, and 4.26% gains in comparison with the advanced Transformer-based method [31] on OA, AA, and  $\kappa$ , respectively. Fig. 6 shows classification predictions, which demonstrates that our S²Mamba realizes the most precise results. For instance, our method is capable of accurately identifying highways (masked in blue color) under shadows, demonstrating its effectiveness.



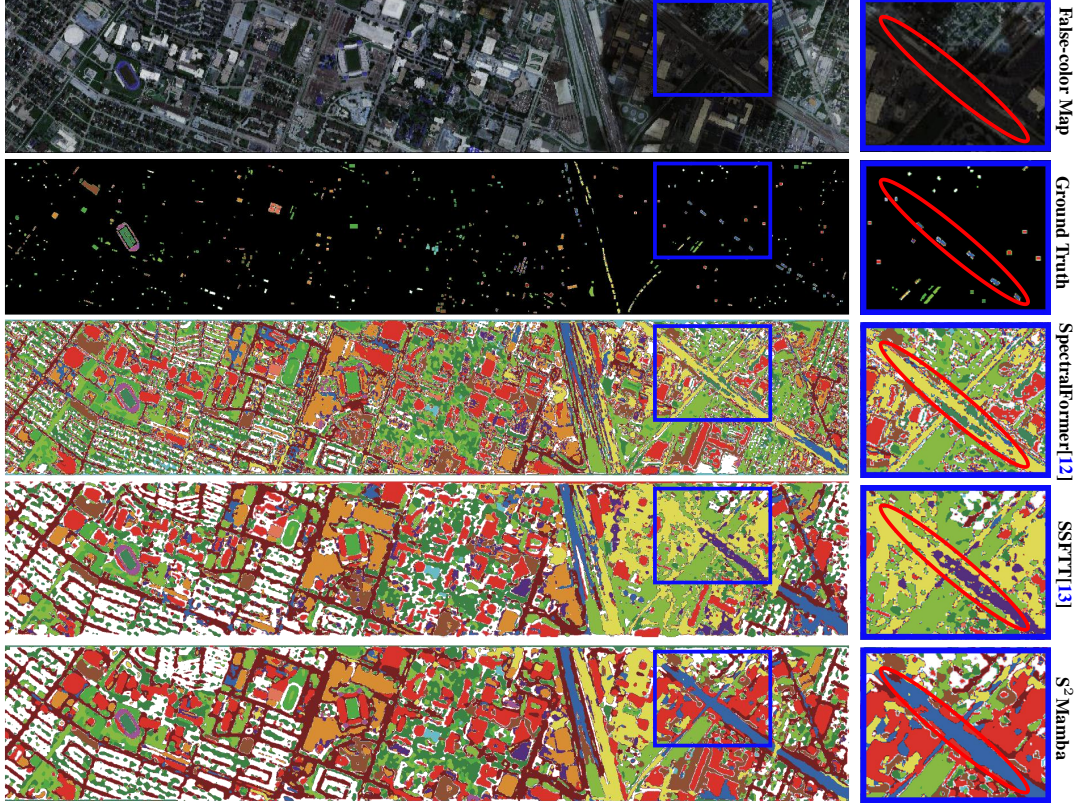


Figure 6: Classification results on the Houston 2013 dataset.

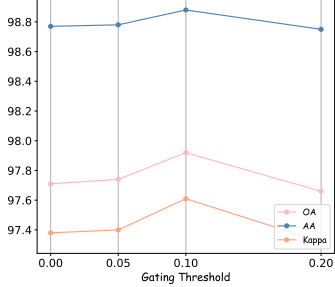


Figure 7: Parameter analysis of different gating thresholds.

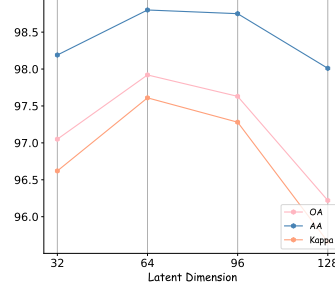


Figure 8: Parameter analysis of different latent dimensions.

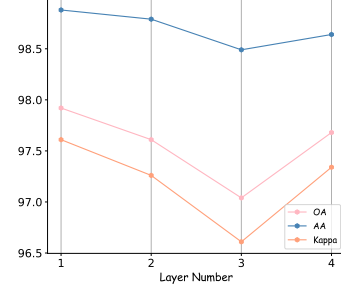


Figure 9: Parameter analysis of different layer numbers.

### 4.3 Ablation Study

**The effectiveness of each component in S<sup>2</sup>Mamba.** We conduct ablation studies in Table 4 to show the impact of each component in S<sup>2</sup>Mamba. The first row shows the performance using the PCS mechanism, which efficiently considers the spatial relations of pixels by a Mamba-based module. As can be seen, it outperforms most comparative methods with 96.45%, 96.42%, and 90.78% OA on Indian Pines, Pavia University, and Houston 2013 datasets, respectively, due to its effective ability in modeling spatial contexts. Then, by incorporating a bi-directional spectral scanning mechanism, we improve performance to 96.72%, 97.17%, and 92.74% OA on the three datasets. This suggests that the BSS can offer more discriminative cues by scanning continuous spectral bands. Finally, by combining both the PCS, BSS, and SMG, we further boost the performance to 97.92%/98.80%/0.9746, 97.81%/97.14%/0.9705, and 93.36%/94.09%/0.9279 in terms of OA/AA/k on the three datasets, which confirms the SMG module can preferably merge spatial and spectral features for each location by a feature competition. The comprehensive results demonstrate that our S<sup>2</sup>Mamba can effectively learn discriminative representations of HSI data.

**Parameter analysis of each component in S<sup>2</sup>Mamba.** We study the effectiveness of hyperparameters in S<sup>2</sup>Mamba, including patch size, gating threshold, latent dimension, and layer numbers. As

shown in Fig. 4, it can be observed that the optimal patch sizes of Indian Pines, Pavia University, and Houston 2013 are 7, 11, and 9, separately, which is consistent with the expectation that the last two datasets comprise more complex spatial boundaries, thereby larger patch inputs are required. Fig. 7 demonstrates that firming the gating threshold to 0.1 can achieve satisfactory results, which can filter those redundant features. Figs. 8 and 9 denote that 64 and 1 are the optimal values of hidden dimension and layer number, respectively. This confirms our S<sup>2</sup>Mamba can achieve state-of-the-art performance with a single-block network, whereas deeper layers or larger hidden dimensions can not yield additional improvements.

## 5 Conclusion

In this paper, we propose S<sup>2</sup>Mamba, a novel architecture for hyperspectral image classification. S<sup>2</sup>Mamba comprises a Patch Cross Scanning mechanism and a Bi-directional Spectral Scanning mechanism for learning the contextual information from spatial and spectral aspects, respectively, which utilize the selective structured state space models as alternatives to self-attention mechanisms for capturing long-range dependency with linear complexity, thereby efficiently improving the results. Furthermore, to optimally merge the above features, a Spatial-spectral Mixture Gate is proposed to adjust the fusion ratio for each position with learnable matrices, further enhancing the classification performance. Experimental results on three datasets verify the superiority of our S<sup>2</sup>Mamba.

## References

- [1] Maryam Imani and Hassan Ghassemian. An overview on spectral and spatial information fusion for hyperspectral image classification: Current trends and challenges. *Information fusion*, 59:59–83, 2020.
- [2] Behnood Rasti, Danfeng Hong, Renlong Hang, Pedram Ghamisi, Xudong Kang, Jocelyn Chanussot, and Jon Atli Benediktsson. Feature extraction for hyperspectral imagery: The evolution from shallow to deep: Overview and toolbox. *IEEE Geoscience and Remote Sensing Magazine*, 8(4):60–88, 2020.
- [3] Shutao Li, Weiwei Song, Leyuan Fang, Yushi Chen, Pedram Ghamisi, and Jon Atli Benediktsson. Deep learning for hyperspectral image classification: An overview. *IEEE Transactions on Geoscience and Remote Sensing*, 57(9):6690–6709, 2019.
- [4] Danfeng Hong, Bing Zhang, Xuyang Li, Yuxuan Li, Chenyu Li, Jing Yao, Naoto Yokoya, Hao Li, Pedram Ghamisi, Xiuping Jia, et al. Spectralgpt: Spectral remote sensing foundation model. *IEEE Transactions on Pattern Analysis and Machine Intelligence*, 2024.
- [5] Antonio Plaza, Jon Atli Benediktsson, Joseph W Boardman, Jason Brazile, Lorenzo Bruzzone, Gustavo Camps-Valls, Jocelyn Chanussot, Mathieu Fauvel, Paolo Gamba, Anthony Gualtieri, et al. Recent advances in techniques for hyperspectral image processing. *Remote sensing of environment*, 113:S110–S122, 2009.
- [6] Xiangrong Zhang, Shunli Tian, Guanchun Wang, Xu Tang, Jie Feng, and Licheng Jiao. Cast: A cascade spectral aware transformer for hyperspectral image change detection. *IEEE Transactions on Geoscience and Remote Sensing*, 2023.
- [7] Yonghao Xu, Bo Du, Fan Zhang, and Liangpei Zhang. Hyperspectral image classification via a random patches network. *ISPRS journal of photogrammetry and remote sensing*, 142:344–357, 2018.
- [8] Zilong Zhong, Jonathan Li, Zhiming Luo, and Michael Chapman. Spectral–spatial residual network for hyperspectral image classification: A 3-d deep learning framework. *IEEE Transactions on Geoscience and Remote Sensing*, 56(2):847–858, 2017.
- [9] Mercedes E Paoletti, Juan Mario Haut, Javier Plaza, and Antonio Plaza. A new deep convolutional neural network for fast hyperspectral image classification. *ISPRS journal of photogrammetry and remote sensing*, 145:120–147, 2018.
- [10] Yanni Dong, Quanwei Liu, Bo Du, and Liangpei Zhang. Weighted feature fusion of convolutional neural network and graph attention network for hyperspectral image classification. *IEEE Transactions on Image Processing*, 31:1559–1572, 2022.

- [11] Danfeng Hong, Lianru Gao, Jing Yao, Bing Zhang, Antonio Plaza, and Jocelyn Chanussot. Graph convolutional networks for hyperspectral image classification. *IEEE Transactions on Geoscience and Remote Sensing*, 59(7):5966–5978, 2020.
- [12] Danfeng Hong, Zhu Han, Jing Yao, Lianru Gao, Bing Zhang, Antonio Plaza, and Jocelyn Chanussot. Spectralformer: Rethinking hyperspectral image classification with transformers. *IEEE Transactions on Geoscience and Remote Sensing*, 60:1–15, 2021.
- [13] Le Sun, Guangrui Zhao, Yuhui Zheng, and Zebin Wu. Spectral–spatial feature tokenization transformer for hyperspectral image classification. *IEEE Transactions on Geoscience and Remote Sensing*, 60:1–14, 2022.
- [14] Swalpa Kumar Roy, Ankur Deria, Chiranjibi Shah, Juan M Haut, Qian Du, and Antonio Plaza. Spectral–spatial morphological attention transformer for hyperspectral image classification. *IEEE Transactions on Geoscience and Remote Sensing*, 61:1–15, 2023.
- [15] Haoyang Yu, Zhen Xu, Ke Zheng, Danfeng Hong, Hao Yang, and Meiping Song. Mstnet: A multilevel spectral–spatial transformer network for hyperspectral image classification. *IEEE Transactions on Geoscience and Remote Sensing*, 60:1–13, 2022.
- [16] Lianhui Liang, Ying Zhang, Shaoquan Zhang, Jun Li, Antonio Plaza, and Xudong Kang. Fast hyperspectral image classification combining transformers and simam-based cnns. *IEEE Transactions on Geoscience and Remote Sensing*, 2023.
- [17] Xiaofei Yang, Weijia Cao, Yao Lu, and Yicong Zhou. Hyperspectral image transformer classification networks. *IEEE Transactions on Geoscience and Remote Sensing*, 60:1–15, 2022.
- [18] Ashish Vaswani, Noam Shazeer, Niki Parmar, Jakob Uszkoreit, Llion Jones, Aidan N Gomez, Łukasz Kaiser, and Illia Polosukhin. Attention is all you need. *Advances in neural information processing systems*, 30, 2017.
- [19] Alexey Dosovitskiy, Lucas Beyer, Alexander Kolesnikov, Dirk Weissenborn, Xiaohua Zhai, Thomas Unterthiner, Mostafa Dehghani, Matthias Minderer, Georg Heigold, Sylvain Gelly, et al. An image is worth 16x16 words: Transformers for image recognition at scale. In *International Conference on Learning Representations*, 2020.
- [20] Albert Gu and Tri Dao. Mamba: Linear-time sequence modeling with selective state spaces. *arXiv preprint arXiv:2312.00752*, 2023.
- [21] Lianghui Zhu, Bencheng Liao, Qian Zhang, Xinlong Wang, Wenyu Liu, and Xinggang Wang. Vision mamba: Efficient visual representation learning with bidirectional state space model. *arXiv preprint arXiv:2401.09417*, 2024.
- [22] Yue Liu, Yunjie Tian, Yuzhong Zhao, Hongtian Yu, Lingxi Xie, Yaowei Wang, Qixiang Ye, and Yunfan Liu. Vmamba: Visual state space model. *arXiv preprint arXiv:2401.10166*, 2024.
- [23] Xiaohuan Pei, Tao Huang, and Chang Xu. Efficientvmamba: Atrous selective scan for light weight visual mamba. *arXiv preprint arXiv:2403.09977*, 2024.
- [24] Keyan Chen, Bowen Chen, Chenyang Liu, Wenyan Li, Zhengxia Zou, and Zhenwei Shi. Rsmamba: Remote sensing image classification with state space model. *arXiv preprint arXiv:2403.19654*, 2024.
- [25] Jun Ma, Feifei Li, and Bo Wang. U-mamba: Enhancing long-range dependency for biomedical image segmentation. *arXiv preprint arXiv:2401.04722*, 2024.
- [26] Sijie Zhao, Hao Chen, Xueliang Zhang, Pengfeng Xiao, Lei Bai, and Wanli Ouyang. Rs-mamba for large remote sensing image dense prediction. *arXiv preprint arXiv:2404.02668*, 2024.
- [27] Zhaohu Xing, Tian Ye, Yijun Yang, Guang Liu, and Lei Zhu. Segmamba: Long-range sequential modeling mamba for 3d medical image segmentation. *arXiv preprint arXiv:2401.13560*, 2024.
- [28] Kunchang Li, Xinhao Li, Yi Wang, Yanan He, Yali Wang, Limin Wang, and Yu Qiao. Video-mamba: State space model for efficient video understanding. *arXiv preprint arXiv:2403.06977*, 2024.
- [29] Dingkan Liang, Xin Zhou, Xinyu Wang, Xingkui Zhu, Wei Xu, Zhikang Zou, Xiaoqing Ye, and Xiang Bai. Pointmamba: A simple state space model for point cloud analysis. *arXiv preprint arXiv:2402.10739*, 2024.

- [30] Renlong Hang, Qingshan Liu, Danfeng Hong, and Pedram Ghamisi. Cascaded recurrent neural networks for hyperspectral image classification. *IEEE Transactions on Geoscience and Remote Sensing*, 57(8):5384–5394, 2019.
- [31] Mengying Jiang, Yuanchao Su, Lianru Gao, Antonio Plaza, Xi-Le Zhao, Xu Sun, and Guizhong Liu. Graphgst: Graph generative structure-aware transformer for hyperspectral image classification. *IEEE Transactions on Geoscience and Remote Sensing*, 2024.
- [32] Haokui Zhang, Ying Li, Yenan Jiang, Peng Wang, Qiang Shen, and Chunhua Shen. Hyperspectral classification based on lightweight 3-d-cnn with transfer learning. *IEEE Transactions on Geoscience and Remote Sensing*, 57(8):5813–5828, 2019.
- [33] Gong Cheng, Zhenpeng Li, Junwei Han, Xiwen Yao, and Lei Guo. Exploring hierarchical convolutional features for hyperspectral image classification. *IEEE Transactions on Geoscience and Remote Sensing*, 56(11):6712–6722, 2018.
- [34] Weiwei Song, Shutao Li, Leyuan Fang, and Ting Lu. Hyperspectral image classification with deep feature fusion network. *IEEE Transactions on Geoscience and Remote Sensing*, 56(6):3173–3184, 2018.
- [35] Swalpa Kumar Roy, Gopal Krishna, Shiv Ram Dubey, and Bidyut B Chaudhuri. Hybridsn: Exploring 3-d–2-d cnn feature hierarchy for hyperspectral image classification. *IEEE Geoscience and Remote Sensing Letters*, 17(2):277–281, 2019.
- [36] Juan Mario Haut, Mercedes E Paoletti, Javier Plaza, Antonio Plaza, and Jun Li. Hyperspectral image classification using random occlusion data augmentation. *IEEE Geoscience and Remote Sensing Letters*, 16(11):1751–1755, 2019.
- [37] Wei Zhao, Licheng Jiao, Wenping Ma, Jiaqi Zhao, Jin Zhao, Hongying Liu, Xianghai Cao, and Shuyuan Yang. Superpixel-based multiple local cnn for panchromatic and multispectral image classification. *IEEE Transactions on Geoscience and Remote Sensing*, 55(7):4141–4156, 2017.
- [38] Shiqi Yu, Sen Jia, and Chunyan Xu. Convolutional neural networks for hyperspectral image classification. *Neurocomputing*, 219:88–98, 2017.
- [39] Lichao Mou, Xiaoqiang Lu, Xuelong Li, and Xiao Xiang Zhu. Nonlocal graph convolutional networks for hyperspectral image classification. *IEEE Transactions on Geoscience and Remote Sensing*, 58(12):8246–8257, 2020.
- [40] Sheng Wan, Chen Gong, Ping Zhong, Shirui Pan, Guangyu Li, and Jian Yang. Hyperspectral image classification with context-aware dynamic graph convolutional network. *IEEE Transactions on Geoscience and Remote Sensing*, 59(1):597–612, 2020.
- [41] Zhuo Zheng, Yanfei Zhong, Ailong Ma, and Liangpei Zhang. Fpga: Fast patch-free global learning framework for fully end-to-end hyperspectral image classification. *IEEE Transactions on Geoscience and Remote Sensing*, 58(8):5612–5626, 2020.
- [42] Xiangrong Zhang, Shouwang Shang, Xu Tang, Jie Feng, and Licheng Jiao. Spectral partitioning residual network with spatial attention mechanism for hyperspectral image classification. *IEEE transactions on geoscience and remote sensing*, 60:1–14, 2021.
- [43] Lichao Mou, Pedram Ghamisi, and Xiao Xiang Zhu. Deep recurrent neural networks for hyperspectral image classification. *IEEE Transactions on Geoscience and Remote Sensing*, 55(7):3639–3655, 2017.
- [44] Atharva Sharma, Xiuwen Liu, and Xiaojun Yang. Land cover classification from multi-temporal, multi-spectral remotely sensed imagery using patch-based recurrent neural networks. *Neural Networks*, 105:346–355, 2018.
- [45] Xin He, Yushi Chen, and Zhouhan Lin. Spatial-spectral transformer for hyperspectral image classification. *Remote Sensing*, 13(3):498, 2021.
- [46] Chunhui Zhao, Boao Qin, Shou Feng, Wenxiang Zhu, Weiwei Sun, Wei Li, and Xiuping Jia. Hyperspectral image classification with multi-attention transformer and adaptive superpixel segmentation-based active learning. *IEEE Transactions on Image Processing*, 2023.
- [47] Zhao Qiu, Jie Xu, Jiangtao Peng, and Weiwei Sun. Cross-channel dynamic spatial-spectral fusion transformer for hyperspectral image classification. *IEEE Transactions on Geoscience and Remote Sensing*, 2023.

- [48] Weilian Zhou, Sei-Ichiro Kamata, Haipeng Wang, and Xi Xue. Multiscanning-based rnn-transformer for hyperspectral image classification. *IEEE Transactions on Geoscience and Remote Sensing*, 2023.
- [49] Albert Gu, Tri Dao, Stefano Ermon, Atri Rudra, and Christopher Ré. Hippo: Recurrent memory with optimal polynomial projections. *Advances in neural information processing systems*, 33:1474–1487, 2020.
- [50] Albert Gu, Karan Goel, and Christopher Re. Efficiently modeling long sequences with structured state spaces. In *International Conference on Learning Representations*, 2021.
- [51] Albert Gu, Isys Johnson, Karan Goel, Khaled Saab, Tri Dao, Atri Rudra, and Christopher Ré. Combining recurrent, convolutional, and continuous-time models with linear state space layers. *Advances in neural information processing systems*, 34:572–585, 2021.
- [52] Jimmy TH Smith, Andrew Warrington, and Scott Linderman. Simplified state space layers for sequence modeling. In *The Eleventh International Conference on Learning Representations*, 2022.
- [53] Ankit Gupta, Albert Gu, and Jonathan Berant. Diagonal state spaces are as effective as structured state spaces. *Advances in Neural Information Processing Systems*, 35:22982–22994, 2022.
- [54] Jiacheng Ruan and Suncheng Xiang. Vm-unet: Vision mamba unet for medical image segmentation. *arXiv preprint arXiv:2402.02491*, 2024.
- [55] Jiarun Liu, Hao Yang, Hong-Yu Zhou, Yan Xi, Lequan Yu, Yizhou Yu, Yong Liang, Guangming Shi, Shaoting Zhang, Hairong Zheng, et al. Swin-umamba: Mamba-based unet with imagenet-based pretraining. *arXiv preprint arXiv:2402.03302*, 2024.
- [56] Guo Chen, Yifei Huang, Jilan Xu, Baoqi Pei, Zhe Chen, Zhiqi Li, Jiahao Wang, Kunchang Li, Tong Lu, and Limin Wang. Video mamba suite: State space model as a versatile alternative for video understanding. *arXiv preprint arXiv:2403.09626*, 2024.
- [57] Xuanhua He, Ke Cao, Keyu Yan, Rui Li, Chengjun Xie, Jie Zhang, and Man Zhou. Pan-mamba: Effective pan-sharpening with state space model. *arXiv preprint arXiv:2402.12192*, 2024.
- [58] Hongruixuan Chen, Jian Song, Chengxi Han, Junshi Xia, and Naoto Yokoya. Changemamba: Remote sensing change detection with spatio-temporal state space model. *arXiv preprint arXiv:2404.03425*, 2024.
- [59] Ilya Loshchilov and Frank Hutter. Decoupled weight decay regularization. In *International Conference on Learning Representations*, 2018.